Vertical Divergence of the Atmospheric Momentum Flux near the Sea Surface at a Coastal Site

L. MAHRT,[a] ERIK NILSSON,[b] ANNA RUTGERSSON,[b] AND HEIDI PETTERSSON[c]

[a] *Northwest Research Associates, Corvallis, Oregon*
[b] *Department of Earth Sciences, Uppsala University, Uppsala, Sweden*
[c] *Finnish Meteorological Institute, Helsinki, Finland*

(Manuscript received 12 April 2021, in final form 16 August 2021)

ABSTRACT: Motivated by previous studies, we examine the underestimation of the sea surface stress due to the stress divergence between the surface and the atmospheric observational level. We analyze flux measurements collected over a 6-yr period at a coastal tower in the Baltic Sea encompassing a wide range of fetch values. Results are posed in terms of the vertical divergence of the stress scaled by the stress at the lowest observational level. The magnitude of this relative stress divergence increases with increasing stability and decreases with increasing instability, possibly partly due to the impact of stability on the boundary layer depth. The magnitude of the relative stress divergence increases modestly with decreasing wave age. The divergence of the heat flux is not well correlated with the divergence of the momentum flux evidently due to the greater influence of advection on the temperature. Needed improvement of the conceptual framework and needed additional measurements are noted.

SIGNIFICANCE STATEMENT: Flux measurements over the sea are typically made at 10 m above the surface. However, the vertical flux divergence measured between two levels suggests that the variation of the surface fluxes and the 10-m fluxes may be significant such that the observed flux at 10 m can seriously underestimate the surface fluxes. This underestimation is documented from long-term flux measurements from a tower in the coastal zone of the Baltic.

KEYWORDS: Air-sea interaction; Momentum; Stress; Surface fluxes

1. Introduction

The stress magnitude in the atmosphere can decrease significantly with height immediately above the sea surface (Miller 1998; Ström and Tjernström 2004; Fairall et al. 2006) such that the stress measured at standard atmospheric observation levels may be significantly smaller than the surface stress. Mahrt et al. (2018a) used linear extrapolation and found that the 10-m fluxes underestimated the surface stress by typically 20% with considerable variation. Stable boundary layers may be particularly thin because reduced downward mixing leads to lower wind speeds at the surface and subsequently smaller surface roughness (Smedman et al. 1997; Mahrt et al. 2001b). A comprehensive study by Ortiz-Suslow et al. (2021) found that the vertical divergence of the momentum flux was more likely to be significant compared to the vertical divergence of the heat and moisture fluxes. They estimated that the momentum flux divergence could be neglected for less than 1/3 of the observations depending on stability and swell orientation. Widespread underestimation of the surface stress could have systematically contaminated calibration of existing surface similarity theory for predicting the surface stress.

The vertical divergence of the heat flux does not necessarily correlate with the momentum flux divergence partly because the momentum flux divergence might be significantly affected by the height dependence of the horizontal pressure gradient in addition to advection of momentum (Fairall et al. 2006). In contrast, the heat flux profile can be controlled by temperature advection and sometimes entrainment fluxes at the top of the boundary layer.

Grachev et al. (2005) examined the momentum and heat flux divergence over sea ice during the polar night with very large fetch and found greater relative stress divergence compared to the relative heat flux divergence [Eqs. (5) and (6)]. For very stable conditions over land, Mahrt et al. (2018b) found significant stress divergence generally associated with boundary layer depths of less than 50 m. But the flux profiles for very stable conditions can also be rather complex because layers of momentum flux convergence and heat flux convergence appear to be common in very stable conditions over land. Wyngaard (2010) derived a general relationship of the depth of the ‘‘constant’’ flux layer to the boundary layer depth, which can be used to estimate when the vertical flux divergence can be neglected.

Thin internal boundary layers are common in offshore flow (Garratt and Ryan 1989; Rogers et al. 1995; Vickers et al. 2001; Sun et al. 2001; Skyllingstad et al. 2005; Dörenkämper et al. 2015). With flow of warm air over cooler water, the stable internal boundary layer may be sufficiently thin that the surface layer lies below typical observational levels (Fairall et al. 2006; Mahrt et al. 2016) and the measurements at the usual levels may significantly underestimate the surface stress. For short-fetch offshore flow over cold water, the downward momentum flux may increase with height due to overlying advected turbulence from land and near collapse of the turbulence near the surface (Vickers et al. 2001; Mahrt et al. 2001a). Then the stress can increase with height and the observed 10-m stress overestimates the surface stress

Corresponding author: L. Mahrt, mahrt@nwra.com

DOI: 10.1175/JPO-D-21-0081.1

magnitude, although this scenario may be uncommon. Formation of a low-level jet in offshore flow can also lead to elevated generation of turbulence that significantly influences the flux near the surface (Smedman et al. 1995). Because observations are limited over the sea, internal boundary layers in offshore flow are less understood than internal boundary layers triggered by onshore flow over land, depending on the complexity of the land surface (Grachev et al. 2018). Distortion of the flux profiles may also be significant when forced by less concentrated changes of the wind vector or SST over open ocean conditions (Samelson et al. 2006; de Szoeke et al. 2017; Skyllingstad et al. 2019; Samelson 2020).

The behavior of the stress becomes more complicated when wave effects are important (Rieder et al. 1994; Rieder and Smith 1998; Drennan et al. 1999; Grachev et al. 2003; Sullivan et al. 2008; Grachev et al. 2011; Nilsson et al. 2012; Hristov and Ruiz-Plancarte 2014; Patton et al. 2019), particularly with low wind speeds and nonstationarity. On the other hand, information on the wave state is generally not required for predicting the surface stress for sufficiently long fetch partly because variation of the wave state becomes highly correlated with the wind speed (Edson et al. 2013). Based on a case study period, Smedman et al. (2009) found that the momentum flux divergence was greatest with wind following swell, of unknown generality. The influence of the wave-induced distortion of the wind profile may reach the 10-m level with swell and low wind speeds (Sullivan and McWilliams 2014). In addition, shoaling and steering of waves induced by the bathymetry can influence the wave-direction statistics and surface stress (Pettersson et al. 2010).

In our study, we examine the dependence of the stress divergence on stability and the resulting underestimation of the surface stress. In section 2, we introduce the measurements and flux partitioning. The relative stress divergence and depth scales are defined in section 3. We then examine the relation of the relative stress divergence to stability (section 4) and wave state (section 5). We briefly investigate the heat flux divergence in section 6.

2. Measurements

We analyze measurements from the Östergarnsholm mast beginning in July 2013 and ending in August 2019, and focus on the Campbell CSAT sonic anemometers located at 10 and 26 m. Maps of the site include Figs. 1–2 in Rutgersson et al. (2001), Fig. 1 in Smedman et al. (2009), and Fig. 1 in Gutiérrez-Loza et al. (2019). For the current study, see Fig. 1. The observational site is described by Smedman et al. (1999), Rutgersson et al. (2001), Sahlée et al. (2008), Högström et al. (2008), and Rutgersson et al. (2020) and citations therein. The potential influence of the local bathymetry and the presence of the low flat island to the north (2 km across) were also discussed. Fluxes measured at the mast compared well with buoy measurements offshore for the open-sea wind directions (e.g., Högström et al. 2008). Because transducer shadow errors for CSAT sonic anemometers (Horst et al. 2015) partially cancel when computing the difference of $\overline{w'u'}$ between levels, we have not attempted to correct for the transducer shadow errors.

The current study also analyzes wave measurements from a Directional Waverider operated by the Finnish Meteorological Institute. The wave buoy is located approximately 4 km southeast from the Östergarnsholm mast where the water depth is 39 m. We divide the wind direction into sectors based on the fetch and bathymetry (Rutgersson et al. 2020). For the northeasterly wind direction (40°–80°), the fetch averages about 220 km. For the southeasterly wind direction (80°–160°), the fetch ranges from 130 to 250 km. The southerly flow sector 160°–220° is the most common direction and the fetch is near 300 km. The fetch is short for westerly direction, 220°–295° with values as small as 4 km. The remaining broad northerly sector contains a mixture of land and sea.

The flow variables are decomposed as

$$\phi = \phi' + \overline{\phi}, \tag{1}$$

where ϕ is potential temperature or one of the velocity components and ϕ' is the deviation from a local time average over 10 min, $\overline{\phi}$. For example, the along-wind momentum flux is written as $\overline{w'u'}$ and the heat flux is written as $\overline{w'\theta'}$. The wind speed is computed as

$$U \equiv \sqrt{\overline{u}^2 + \overline{v}^2}. \tag{2}$$

3. Stress divergence

a. Definitions

The stress divergence is estimated as

$$\delta_z \overline{w'u'} \equiv C(\overline{w'u'_2} - \overline{w'u'_1}), \tag{3}$$

where $\overline{w'u'_1}$ and $\overline{w'u'_2}$ are the momentum fluxes at 10 and 26 m, respectively, and C = 10 m/16 m converts the vertical difference of the momentum flux to an estimate for a 10-m layer using a local linear height dependence. This provides some measure of standardization independent of the particular measurement levels for this site. Adding $-\delta_z\overline{w'u'}$ to the 10-m flux estimates the surface stress. In this study, we examine the behavior of $\delta_z\overline{w'u'}$. If the magnitude of the downward momentum flux decreases with height, then $\delta_z\overline{w'u'}$ is positive so that the flux divergence term in the momentum equation is negative, as in a normal boundary layer. We also compute

$$\delta_z \overline{w'T'} \equiv C(\overline{w'T'_2} - \overline{w'T'_1}). \tag{4}$$

Negative values of $\delta_z\overline{w'T'}$ correspond to the usual vertical convergence of the upward heat flux in the unstable boundary layer and the usual divergence of the downward heat flux in the stable boundary.

Similar to the calculations of Grachev et al. (2005), we additionally compute the relative divergence of the momentum flux

$$\frac{\delta_z \overline{w'u'}}{\overline{w'u'}}. \tag{5}$$

The relative divergence of the momentum flux is normally negative because $\delta_z\overline{w'u'}$ is generally positive and $\overline{w'u'}$ is usually negative. The relative heat flux divergence is

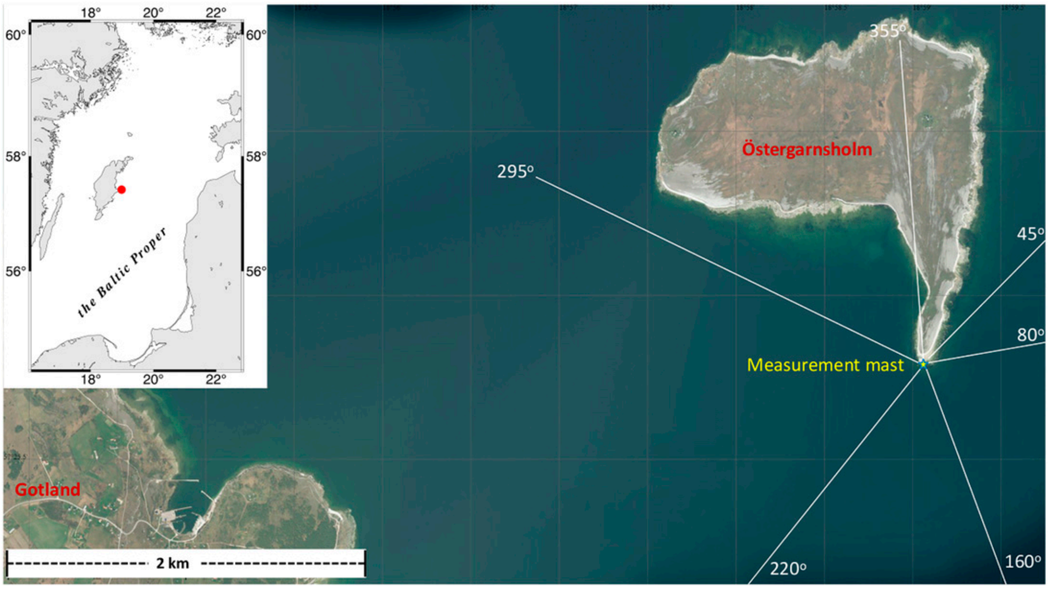

FIG. 1. The map of the local site and the inset were generated using GMT 6 (Wessel et al. 2019). The aerial photograph was adapted from https://map.openseamap.org/ and the OpenStreetMap-Project (CC-BY-SA 2.0).

$$\frac{\delta_z \overline{w'T'}}{\overline{w'T'}}. \tag{6}$$

Our analyses will generally be based on bin averaging quantities in terms of intervals of z/L designated with square brackets, for example $[\overline{w'u'}]$. The term L is the Obukhov length, and z is the height above the sea surface. Ratios are computed in terms of bin-averaged quantities to obtain $[\delta_z \overline{w'u'}]/[\overline{w'u'}]$. Most of the bins include a large number of data points so that the standard error is generally small and difficult to visualize. However, the uncertainty of the bin averages is probably substantially underestimated by the standard error because the samples are not independent due to nonstationarity.

b. Depth scale

A depth scale for the momentum flux divergence can be written as

$$h_{wu} \equiv -\frac{[\overline{w'u'}]}{\delta_z[\overline{w'u'}]/\delta z}. \tag{7}$$

A similar expression can be written for the depth scale of the heat flux divergence $h_{w\theta}$. If the fluxes decrease linearly with height and approximately vanish at the boundary layer top, then h_{wu} and $h_{w\theta}$ are estimates of the boundary layer depth. Direct estimates of boundary layer depth are not available for this dataset. If we expect both the momentum flux and the heat flux to approximately vanish at the true boundary layer top, then the observed significant differences between h_{wu} and $h_{w\theta}$ indicate that the low-level flux profiles are not reliable estimates of the boundary layer depth. The stress divergence tends to decrease with height within the boundary layer at the Östergarnsholm site, as shown in Fig. 10b of Svensson et al. (2019) using momentum fluxes computed from lidar measurements. Thus, h_{wu}, based on near surface observations, may seriously underestimate the boundary layer depth. We consider h_{wu} to be a useful depth scale as the first-order approximation to the near-surface height variation of the turbulent fluxes.

c. Advective balance

The impact of advection on the flux profile is generally more dominant for the heat flux profile compared to the momentum flux profile. For semistationary adiabatic flow, the vertical variation of the heat flux is often controlled by advection so that

$$\mathbf{V} \cdot \nabla\theta \approx -\frac{\partial \overline{w'\theta'}}{\partial z}. \tag{8}$$

Cold-air advection can be balanced by heat-flux convergence such that the upward heat flux decreases with height in the layer of horizontal advection. Warm air advection would be balanced by decreasing downward heat flux with height. In either case, the relative flux divergence [Eq. (6)] is negative. This interpretation assumes that upward heat flux occurs with cold air advection and downward heat flux occurs with warm air advection. As a less common example, both cold air advection and downward heat flux at the surface lead to an increase of the downward heat flux with height which reaches a maximum at some level, perhaps associated with an entrainment zone where the magnitude of the downward heat flux decreases rapidly with height. An analogous maximum occurs with concurrent warm air advection and upward heat flux at the surface.

Vertically integrating Eq. (8) across the boundary layer and assuming that the heat flux vanishes at the boundary layer top, the boundary layer depth can be estimated as

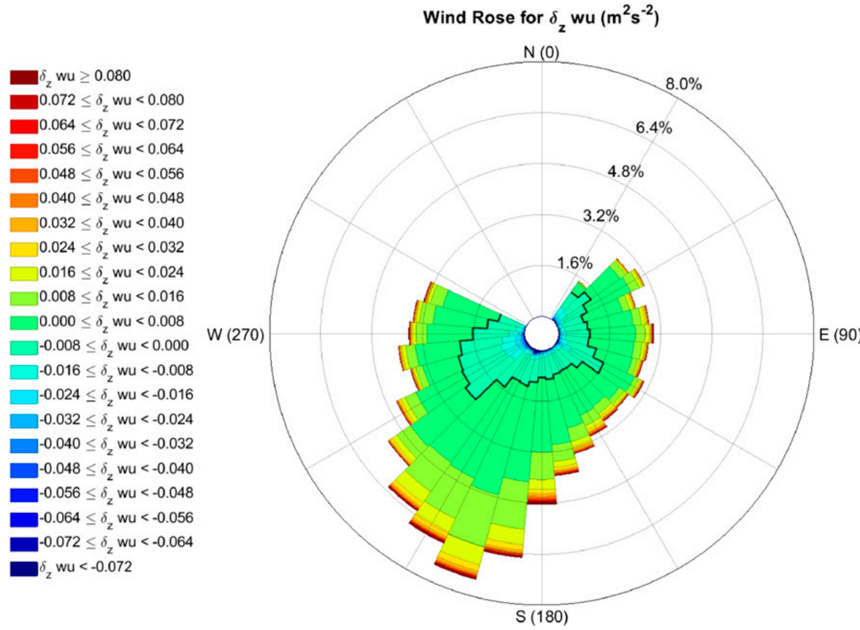

FIG. 2. The relative frequency of the estimated vertical difference of the momentum flux between the 10- and 26-m levels projected onto a 10-m layer [Eq. (3)] for different wind-direction sectors. Positive values generally correspond to decreasing downward momentum flux with height. The color scale describes the sign and magnitude of the vertical difference of the momentum flux and the black boundary partitions the rose into the usual momentum flux divergence (outward from the black boundary) and the momentum flux convergence (inward).

$$h_{w\theta} \approx \frac{\overline{w'\theta'}_{\rm sfc}}{\{\mathbf{V}\cdot\nabla\theta\}}, \tag{9}$$

where $\{\mathbf{V}\cdot\nabla\theta\}$ is the layer-averaged advection of potential temperature. Stronger advection implies a shallower boundary layer. Because the magnitude of the surface heat flux is normally smaller for significantly stable conditions, the corresponding value of $h_{w\theta}$ is smaller for the same magnitude of the advection. Although qualitatively instructive, this relationship requires unavailable estimates of the temperature advection.

4. Dependence on wind direction and stability

The dependence of the frequency distribution of $\delta_z\overline{w'u'}$ [Eq. (3)] on the wind direction (Fig. 2) indicates that the flow from 180° to 220° is dominated by the momentum flux divergence ($\delta_z\overline{w'u'} > 0$, light green to red, outside of the black boundary). Wind directions from 220° to 295° correspond to shorter fetch and greater frequency of the momentum flux convergence $\delta_z\overline{w'u'} < 0$ (blue-green, inside of black boundary), often related to increasing downward momentum flux with height, discussed below. Thus, the behavior of $\delta_z\overline{w'u'}$ at this coastal site depends significantly on the fetch or wind direction.

a. Stability dependence

We composite the relative momentum flux divergence $\delta_z\overline{w'u'}/\overline{w'u'}$ over intervals of the wind direction and intervals of z/L where $z = 10$ and L is based on the 10-m fluxes, as is $\overline{w'u'}$ in the denominator of the relative momentum flux divergence. The stability z/L is contaminated by the difference of the fluxes between the observational level and the surface although here z/L is used only crudely to represent the stability. To compute a bin-averaged value of $\delta_z\overline{w'u'}/\overline{w'u'}$, both $\delta_z\overline{w'u'}$ and $\overline{w'u'}$ are bin averaged independently and then the ratio is computed to avoid very large individual values of the ratio where the magnitude of $\overline{w'u'}$ is particularly small. The magnitude of the relative stress divergence is greatest for stable conditions (Fig. 3). The negative values of $\delta_z[\overline{w'u'}]/[\overline{w'u'}]$ correspond to decreasing downward momentum flux with height, which acts to decelerate the flow, as in a normal boundary layer where the stress divergence and the horizontal pressure gradient oppose each other.

Figure 3b shows the relative momentum flux divergence as a function of an extended range of z/L, which is possible for the southerly wind direction interval 160°–220° where the sample size is largest. The fetch is longest and the magnitude of the relative stress divergence is largest for this wind-direction sector. Near-neutral conditions contain the most data.

The magnitude of the relative stress divergence for the most stable interval of z/L reaches ≈ 0.65 (Fig. 3b, black). This systematic increase of the relative stress divergence with increasing z/L is in agreement with Grachev et al. (2005, their Fig. 2). For a given value of z/L, the magnitude of the relative stress divergence in Grachev et al. (2005, their Fig. 2) was significantly smaller than in Fig. 3b of this study. This difference is at least partly due to computing $\delta_z[\overline{w'u'}]$ over significantly smaller intervals of height in Grachev et al. (2005) compared to the current study.

The magnitude of the relative stress divergence is a little more than 10% for near neutral and unstable conditions. The larger

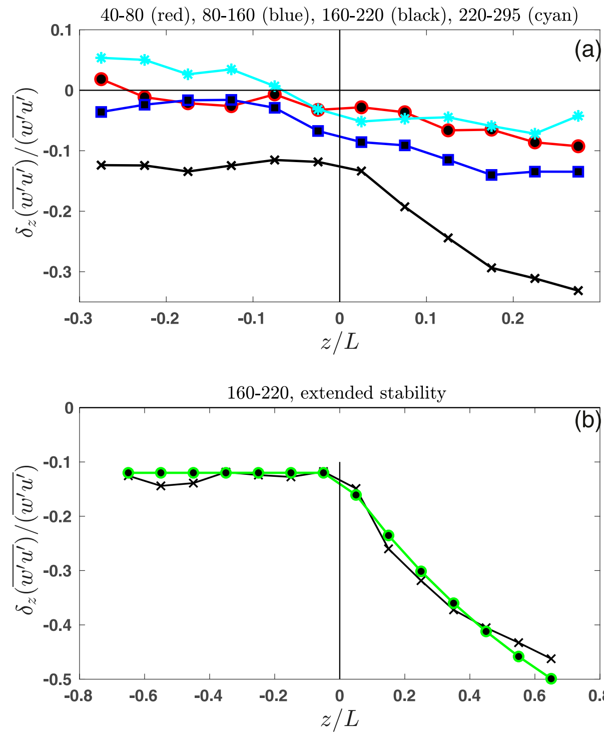

FIG. 3. (a) The relative stress divergence as a function of z/L for different wind-direction sectors. The wind direction intervals are 40°–80° (red circles), 80°–160° (blue squares), 160°–220° (black X marks), and 220°–295° (cyan asterisks). (b) The relative stress divergence for 160°–220° for an extended stability range (black X marks). The other wind direction sectors did not contain sufficient data for this extended range. Also shown is the informal fit [Eq. (10)] for the southerly wind-direction sector (green circles).

composited values of the relative stress divergence for greater fetch are partly due to the persistent positive sign of $\delta_z\overline{w'u'}$ (Fig. 2). Shorter-fetch conditions have numerous cases of negative $\delta_z\overline{w'u'}$ such that the composited values (Fig. 3) are smaller due to sign switching between observations. Only a small percentage of the cases correspond to upward momentum flux so that most of the sign switching of the relative flux divergence is due to changes of $\delta_z\overline{w'u'}$ rather than changes off $\overline{w'u'}$.

Because of the shared variable $\overline{w'u'}$ in Fig. 3, the relationship between the relative flux divergence and z/L is influenced by positive self-correlation. However, the observed correlation is negative and thus not caused by the self-correlation. Estimation of the standard error for $\delta_z[\overline{w'u'}]/[\overline{w'u'}]$ is a little more difficult to interpret because $\delta_z\overline{w'u'}$ and $\overline{w'u'w'u'}$ are composited separately, each having its own standard error.

The significant stress divergence for the unstable case for southerly flow (160°–220°, black curve) might be unexpected because of an anticipated deeper boundary layer for longer-fetch unstable conditions. However, the depth of the convective boundary layer could be constrained by a low-level capping inversion. The frequency distribution of $\delta_z[\overline{w'u'}]$ for the unstable case is quite peaked with few outliers. For southerly flow, $\delta_z\overline{w'u'} < 0$ (flux convergence) occurs for only 17% of the 10-min periods. Thus, the downward momentum flux near the surface decreases with height for most of the unstable cases. Only a few events occur where the stress convergence is persistent for more than a couple of subsequent 10-min periods.

For the other wind directions, events of persistent stress convergence are more common. In general, the decrease of the stress with height is not related to directional shear or crosswind stress. The crosswind stress is mainly important for $U < 2\,\mathrm{m\,s^{-1}}$ and the sign of the crosswind stress is not systematic. For unstable conditions the flux footprint may shrink to the extent that local shoaling becomes important, although there is no evidence that the relative stress divergence is changing significantly with increasing $-z/L$ (Fig. 3). The potential effects of wave state on the flux divergence are discussed in section 5.

The relative stress divergence depends significantly on wind direction for this coastal site. For northeasterly flow, the relative stress divergence is less than 10% even for the most stable conditions (Fig. 3a, red circles). For southeasterly flow (blue squares), the relative stress divergence for unstable conditions is small, similar to that for northeasterly flow. For stable conditions, the magnitude of the relative stress divergence is more significant. For the short-fetch westerly flow, the relative stress convergence $\delta_z[\overline{w'u'}]/[\overline{w'u'}] > 0$ occurs with unstable conditions (cyan asterisks) that would act to accelerate the flow over the sea, probably associated with the decrease of the roughness from land to sea. Elevated advection of more significant turbulence from land may occur at higher levels and lead to an increase of the downward momentum flux with height (flux convergence). Low-level jets at this site (Smedman et al. 1995) generate elevated turbulence and downward transport of turbulence and momentum.

b. Formulation

The relative flux divergence $[\delta_z\overline{w'u'}]/[\overline{w'u'}]$, projected onto a 10-m layer for the 160°–220° wind-direction sector (black, Fig. 3b), is subjectively approximated for stable conditions as (green curve)

$$\delta_z[\overline{w'u'}]/[\overline{w'u'}] = -0.12 - 0.7[1 - \exp(1.2\,z/L)]. \qquad (10)$$

To estimate the surface stress, the predicted $\delta_z[\overline{w'u'}]$ can be added to the 10-m stress $\overline{w'u'}$. For the unstable case, $\delta_z[\overline{w'u'}]/[\overline{w'u'}]$ is approximated as constant equal to 0.12. Although Eq. (10) is oversimplified, it can serve as a basis for evaluating model sensitivity to stress corrections.

5. Wave state

The effect of nonequilibrium wave state is often represented in terms of wave age defined as C_p/u_* or C_p/U where C_p is the wave phase speed at the peak frequency. With long fetch, the wave age C_p/u_* becomes well correlated with U and explicit inclusion of wave age in the prediction of the drag coefficient appears to be unnecessary (Edson et al. 2013). With short fetch, wave age is more likely to be independently important. Although u_*/C_p could be preferable to C_p/U for quantitative examination of the momentum exchange between the wind and wave fields, partitioning the observations according to u_*/C_p for examination of dependencies on z/L corresponds to a form of shared variables (self-correlation) of unknown significance.

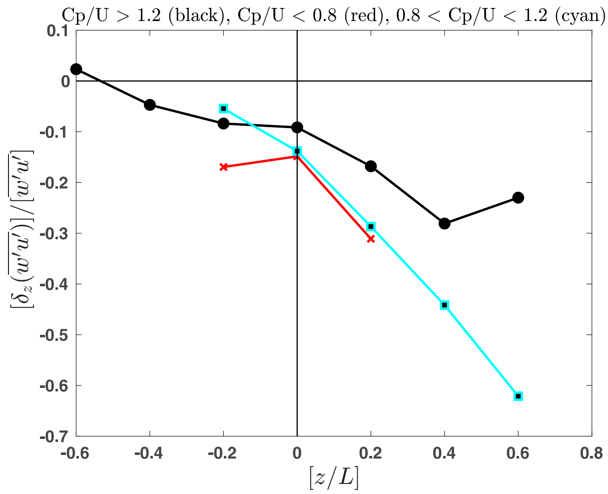

FIG. 4. The relative stress divergence $\delta_z[\overline{w'u'}]/[\overline{w'u'}]$ as a function of z/L for three classes of C_p/U for the wind-direction sector 160°–220°.

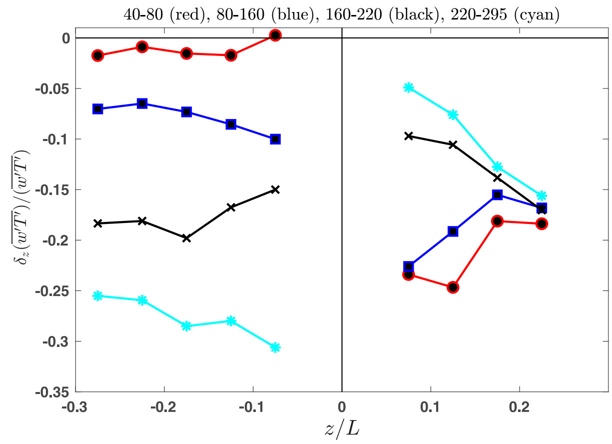

FIG. 5. The relative heat flux divergence for different wind-direction sectors as a function of z/L. The wind direction intervals are 40°–80° (red circles), 80°–160° (blue squares), 160°–220° (black X marks), and 220°–295° (cyan asterisks). For unstable conditions, the upward heat flux decreases with height possibly driven by cold air advection or local warming of the air. For stable conditions, the downward heat flux decreases with height possibly driven by warm air advection or local cooling of the air.

We proceed with use of C_p/U and note that the two forms of wave age are well correlated and the ratio $(C_p/U)/(C_p/u_*)$ is simply the square root of the drag coefficient.

Figure 4 displays $\delta_z[\overline{w'u'}]/[\overline{w'u'}]$ as a function of z/L for three different classes of C_p/U, based on the Directional Waverider buoy. Cases where the dominant wave direction differed by more than 40° from the wind direction were eliminated. Imposing a restriction on the period, such as <6 s, reduces the possibility of long waves shoaling. Such a restriction had little impact on the overall results and was not applied. For southerly flow (160°–220°), approximately 50% of the cases correspond to larger wave age $C_p/U > 1.2$ (swell) and 19% of the cases correspond to smaller wave age $C_p/U < 0.8$ (wind sea); see also Table 2 in Högström et al. (2008).

The magnitude of the relative flux divergence is greatest for small wave age ($C_p/U < 0.8$, red curve, X marks) and smallest for the larger wave age ($C_p/U > 1.2$, black curve, circles). Perhaps the young waves are still developing and the boundary layer depth is smaller than that for more mature waves. The magnitude of $\delta_z[\overline{w'u'}]/[\overline{w'u'}]$ for the intermediate class of wave age (cyan squares) for near neutral conditions is less than that for the large wave age class, although the value for the intermediate wave class is similar to that for small wave-age class. The error bars in Fig. 4 are very small but likely significantly underestimate the uncertainties. The accuracy and generality of Fig. 4 is uncertain.

Representing wave state by wave age C_p/U alone could be a serious oversimplification because of the potential independent importance of other wave characteristics. For example, wave steepness can strongly influence the stress (e.g., Taylor and Yelland 2001; Drennan et al. 2005), although the physics of the impact of wave steepness on $\delta_z[\overline{w'u'}]/[\overline{w'u'}]$ was difficult to isolate. In addition, nonstationarity of the wind field partially decouples the relationship between fetch and wave age. Nonstationarity presumably influences the wave evolution when the wind field changes significantly during the parcel travel time from the coast to the observational site. In general, wave characteristics would lag local time changes of wind field. Even with stationary conditions, curved trajectories can complicate estimation of the fetch.

6. Heat flux divergence

The dependence of the relative heat flux divergence on (z/L) (Fig. 5) omits near-neutral conditions because the heat flux is generally small and calculation of the heat flux divergence becomes unreliable. The magnitude of the relative heat flux divergence varies substantially across the omitted near-neutral regime. For unstable conditions, the relative heat flux divergence is generally negative because the upward heat flux decreases with height ($\delta_z\overline{w'T'} < 0$, $\overline{w'T'} > 0$). For stable conditions, the relative heat flux divergence is also negative because the downward heat flux decreases with height ($\delta_z\overline{w'T'} > 0$, $\overline{w'T'} < 0$).

For the southerly wind direction interval 160°–220° (black X marks), the relative heat flux divergence is 15%–20% for significantly unstable and the most stable conditions. Smaller heat flux divergence would normally be expected for unstable conditions if the boundary layer depth is deeper for unstable conditions and temperature advection is small. Evidently advection is important. Estimation of advection is difficult and can be sensitive to the horizontal scale of the calculation of the horizontal temperature gradient. For northeasterly flow (red circles), the heat flux divergence is near zero for unstable conditions possibly due to deeper boundary layers. The heat flux divergence is significant for stable conditions where the relative flux divergence is about 20%. For the most stable conditions, the relative heat flux divergence for all wind direction groups converges to about 15%–20%, perhaps fortuitously.

For the short-fetch westerly flow (Fig. 5, cyan asterisks), the heat flux convergence is relatively large for unstable conditions (15%–30%, Fig. 5). Thus, the heat flux profile is consistent with a thin unstable internal boundary layer generated by cold-air advection from land. The momentum flux convergence (Fig. 3) is probably associated with the decrease of the roughness from land to sea. Unstable conditions presumably preferentially occur with cold air advection as may occur at night with offshore flow in the coastal zone, or may occur due to larger-scale cold air advection. Stable conditions due to advection of warmer air are more likely in daytime with advection of warm air from land or general synoptic warm air advection.

Comparing Figs. 3 and 5 indicates that the relative flux divergence for heat and momentum are not closely related in spite of being generated by the same turbulence. The heat flux divergence is often controlled by horizontal advection of temperature especially for quasi-stationary conditions. In contrast, the stress divergence is partly controlled by the horizontal pressure gradient and its height dependence.

7. Conclusions

Approximately 6 years of eddy-covariance measurements from two observational levels at the Östergarnsholm site in the Baltic Sea were analyzed to investigate the vertical divergence of the stress. For the current dataset, the relative stress divergence tends to increase with increasing stability and decrease with increasing instability, probably because the boundary layer depths are generally smaller for stable conditions. However, no observations of the boundary layer depth were available. Because of the substantial stress divergence, the magnitude of the surface stress appears to be significantly underestimated by flux observations at standard levels such as 10 m. That is, the calibration of the bulk formula with existing observations is expected, on average, to underestimate the surface stress.

For southerly flow (longest fetch), results are summarized in terms of an informal fit of the relative stress divergence to the stability to provide a basis for model sensitivity studies. Any corrections for the surface stress must be applied with caution because estimating the vertical divergence of the stress is more vulnerable to errors than estimating the stress itself. The averaged relative stress divergence tends to be smaller for short-fetch wind directions because of cases of momentum flux convergence. The magnitude of the stress divergence tends to decrease with increasing wave age, although the generality of this result is not known. The heat flux divergence is not closely related to the divergence of the momentum flux partly due to the important role of temperature advection.

Improved estimates of the stress divergence would benefit from an offshore tower with more flux levels. Ideal deployment would include a flux level closer to the surface that could be mechanically raised with high seas. Measurements of the boundary layer depth would be most useful for further understanding of the factors controlling the stress divergence.

Acknowledgments. We gratefully acknowledge the helpful and important comments from the three anonymous reviewers. Larry Mahrt is funded by Grant N00014-19-1-2469 from the U.S. Office of Naval Research. The Östergarnsholm station is funded by ICOS (Swedish Research Council; Grant No. 2015-06020 and Uppsala University). Erik Nilsson and Anna Rutgersson were partly funded by Swedish Research Council (Grant No. 2015-06020) and FORMAS (Grant No. 2018-01784). The authors are grateful to Marcus Wallin and Leonie Esters for their technical efforts in making measurements at the Östergarnsholm site possible. We thank Mr. Hannu Jokinen at the Finnish Meteorological Institute for assisting with the wave data.

Data availability statement. The data involve different institutions and are not yet available.

REFERENCES

de Szoeke, S. P., E. Skyllingstad, P. Zuidema, and A. S. Chandra, 2017: Cold pools and their influence on the tropical marine boundary layer. *J. Atmos. Sci.*, **74**, 1149–1168, https://doi.org/10.1175/JAS-D-16-0264.1.

Dörenkämper, M., M. Optis, A. Monahan, and G. Steinfeld, 2015: On the offshore advection of boundary-layer structures and the influence on offshore wind conditions. *Bound.-Layer Meteor.*, **155**, 459–482, https://doi.org/10.1007/s10546-015-0008-x.

Drennan, W. M., K. K. Kahma, and M. A. Donelan, 1999: On momentum flux and velocity spectra over waves. *Bound.-Layer Meteor.*, **92**, 489–515, https://doi.org/10.1023/A:1002054820455.

——, P. K. Taylor, and M. J. Yelland, 2005: Parameterizing the sea surface roughness. *J. Phys. Oceanogr.*, **35**, 835–848, https://doi.org/10.1175/JPO2704.1.

Edson, J. B., and Coauthors, 2013: On the exchange of momentum over the open ocean. *J. Phys. Oceanogr.*, **43**, 1589–1610, https://doi.org/10.1175/JPO-D-12-0173.1.

Fairall, C. W., and Coauthors, 2006: Turbulent bulk transfer coefficients and ozone deposition velocity in the International Consortium for Atmospheric Research into Transport and Transformation. *J. Geophys. Res.*, **111**, D23S2, https://doi.org/10.1029/2006JD007597.

Garratt, J., and B. Ryan, 1989: The structure of the stably stratified internal boundary layer in offshore flow over the sea. *Bound.-Layer Meteor.*, **47**, 17–40, https://doi.org/10.1007/BF00122320.

Grachev, A. A., C. W. Fairall, J. E. Hare, J. B. Edson, and S. D. Miller, 2003: Wind stress vector over ocean waves. *J. Phys. Oceanogr.*, **33**, 2408–2429, https://doi.org/10.1175/1520-0485(2003)033<2408:WSVOOW>2.0.CO;2.

——, C. Fairall, P. Persson, E. Andreas, and P. Guest, 2005: Stable boundary-layer scaling regimes: The SHEBA data. *Bound.-Layer Meteor.*, **116**, 201–235, https://doi.org/10.1007/s10546-004-2729-0.

——, L. Bariteau, C. W. Fairall, J. E. Hare, D. Helmig, J. Hueber, and E. K. Lang, 2011: Turbulent fluxes and transfer of trace gases from ship-based measurements during TexAQS 2006. *J. Geophys. Res.*, **116**, D13110, https://doi.org/10.1029/2010JD015502.

Grachev, A., L. S. Leo, H. J. S. Fernando, C. W. Fairall, E. Creegan, B. Blomquist, A. Christman, and C. Hocut, 2018: Air-sea/land interaction in the coastal zone. *Bound.-Layer Meteor.*, **167**, 181–210, https://doi.org/10.1007/s10546-017-0326-2.

Gutiérrez-Loza, L., M. Wallin, E. Sahlée, E. Nilsson, H. W. Bange, A. Kock, and A. Rutgersson, 2019: Measurement of air-sea methane fluxes in the Baltic Sea using the eddy covariance method. *Front. Earth Sci.*, **7**, 93, https://doi.org/10.3389/feart.2019.00093.

Högström, U., and Coauthors, 2008: Momentum fluxes and wind gradients in the marine boundary layer – A multiplatform study. *Boreal Environ. Res.*, **13**, 475–502.

Horst, T. W., S. R. Semmer, and G. Maclean, 2015: Correction of a non-orthogonal, three-component sonic anemometer for flow distortion by transducer shadowing. *Bound.-Layer Meteor.*, **155**, 371–395, https://doi.org/10.1007/s10546-015-0010-3.

Hristov, T., and J. Ruiz-Plancarte, 2014: Dynamic balances in a wavy boundary layer. *J. Phys. Oceanogr.*, **44**, 3185–3194, https://doi.org/10.1175/JPO-D-13-0209.1.

Mahrt, L., D. Vickers, J. Edson, J. Wilczak, J. Hare, and J. Højstrup, 2001a: Vertical structure of turbulence in offshore flow during RASEX. *Bound.-Layer Meteor.*, **100**, 47–61, https://doi.org/10.1023/A:1018982828967.

——, ——, J. Sun, T. L. Crawford, G. Crescenti, and P. Frederickson, 2001b: Surface stress in offshore flow and quasi-frictional decoupling. *J. Geophys. Res.*, **106**, 20 629–20 639, https://doi.org/10.1029/2000JD000159.

——, E. L. Andreas, J. B. Edson, D. Vickers, J. Sun, and E. G. Patton, 2016: Coastal zone surface stress with stable stratification. *J. Phys. Oceanogr.*, **46**, 95–105, https://doi.org/10.1175/JPO-D-15-0116.1.

——, S. Miller, T. Hristov, and J. Edson, 2018a: On estimating the surface wind stress over the sea. *J. Phys. Oceanogr.*, **48**, 1533–1541, https://doi.org/10.1175/JPO-D-17-0267.1.

——, C. K. Thomas, A. A. Grachev, and P. O. G. Persson, 2018b: Near-surface vertical flux divergence in the stable boundary layer. *Bound.-Layer Meteor.*, **169**, 373–393, https://doi.org/10.1007/s10546-018-0379-x.

Miller, S., 1998: The structure of turbulent and wave-induced wind fields over open-ocean waves. Ph.D. thesis, University of California, Irvine, 202 pp.

Nilsson, E., A. Rutgersson, A.-S. Smedman, and P. P. Sullivan, 2012: Convective boundary-layer structure in the presence of wind following swell. *Quart. J. Roy. Meteor. Soc.*, **138**, 1476–1489, https://doi.org/10.1002/qj.1898.

Ortiz-Suslow, D. G., J. Kalogiros, R. Yamaguchi, and Q. Wang, 2021: An evaluation of the constant flux layer in the atmospheric flow above the wavy air-sea interface. *J. Geophys. Res.*, **126**, e2020JD032834, https://doi.org/10.1029/2020JD032834.

Patton, E., P. P. Sullivan, B. Kosović, J. Dudhia, L. Mahrt, M. Žagar, and T. Marić, 2019: On the influence of swell propagation angle on surface drag. *J. Appl. Meteor. Climatol.*, **58**, 1039–1059, https://doi.org/10.1175/JAMC-D-18-0211.1.

Pettersson, H., K. Kahma, and L. Tuomi, 2010: Wave directions in a narrow bay. *J. Phys. Oceanogr.*, **40**, 156–169, https://doi.org/10.1175/2009JPO4220.1.

Rieder, K. F., and J. A. Smith, 1998: Removing wave effects from the wind stress vector. *J. Geophys. Res.*, **103**, 1363–1374, https://doi.org/10.1029/97JC02571.

——, ——, and R. A. Weller, 1994: Observed directional characteristics of the wind, wind stress, and surface waves on the open ocean. *J. Geophys. Res.*, **99**, 22 589–22 596, https://doi.org/10.1029/94JC02215.

Rogers, D. P., D. W. Johnson, and C. A. Friehe, 1995: Stable internal boundary layer over a coastal sea. Part I: Airborne measurements of the mean and turbulence structure. *J. Atmos. Sci.*, **52**, 667–683, https://doi.org/10.1175/1520-0469(1995)052<0684:TSIBLO>2.0.CO;2.

Rutgersson, A., A. Smedman, and A. Omstedt, 2001: Measured and simulated latent and sensible heat fluxes at two marine sites in the Baltic Sea. *Bound.-Layer Meteor.*, **99**, 53–84, https://doi.org/10.1023/A:1018799227854.

——, and Coauthors, 2020: Using land-based stations for air-sea interaction studies. *Tellus*, **72A**, 1–23, https://doi.org/10.1080/16000870.2019.1697601.

Sahlée, E., A. Smedman, U. Högström, and A. Rutgersson, 2008: Re-evaluation of the bulk exchange coefficient for humidity at sea during unstable and neutral conditions. *J. Phys. Oceanogr.*, **38**, 257–272, https://doi.org/10.1175/2007JPO3754.1.

Samelson, R. M., 2020: Surface stress and atmospheric boundary layer response to mesoscale SST structure in coupled simulations of the northern California Current System. *Mon. Wea. Rev.*, **148**, 259–287, https://doi.org/10.1175/MWR-D-19-0200.1.

——, E. D. Skyllingstad, D. B. Chelton, S. K. Esbensen, L. W. O'Niell, and N. Thum, 2006: On the coupling of wind stress and sea surface temperature. *J. Climate*, **19**, 1557–1566, https://doi.org/10.1175/JCLI3682.1.

Skyllingstad, E. D., R. M. Samelson, L. Mahrt, and P. Barbour, 2005: A numerical modeling study of warm offshore flow over cool water. *Mon. Wea. Rev.*, **133**, 345–361, https://doi.org/10.1175/MWR-2845.1.

——, S. de Zoecke, and L. O'Neill, 2019: Modeling the transient response of tropical convection to mesoscale SST variations. *J. Atmos. Sci.*, **76**, 1227–1244, https://doi.org/10.1175/JAS-D-18-0079.1.

Smedman, A.-S., H. Bergström, and U. Högström, 1995: Spectra, variances and length scales in a marine stable boundary layer dominated by a low level jet. *Bound.-Layer Meteor.*, **76**, 211–232, https://doi.org/10.1007/BF00709352.

——, U. Högström, and H. Bergström, 1997: The turbulence regime of a very stable marine airflow with quasi-frictional decoupling. *J. Geophys. Res.*, **102**, 21 049–21 059, https://doi.org/10.1029/97JC01070.

——, ——, ——, A. Rutgersson, K. Kahma, and H. Pettersson, 1999: A case study of air-sea interaction during swell conditions. *J. Geophys. Res.*, **104**, 25 833–25 851, https://doi.org/10.1029/1999JC900213.

——, ——, E. Sahlée, W. M. Drennan, K. K. Kahma, and H. Pettersson, 2009: Observational study of marine atmospheric boundary layer characteristics during swell. *J. Atmos. Sci.*, **66**, 2747–2763, https://doi.org/10.1175/2009JAS2952.1.

Ström, L., and M. Tjernström, 2004: Variability in the summertime coastal marine atmospheric boundary-layer off California, USA. *Quart. J. Roy. Meteor. Soc.*, **130**, 423–448, https://doi.org/10.1256/qj.03.12.

Sullivan, P. P., and J. C. McWilliams, 2014: Large-eddy simulation of marine atmospheric boundary layers above a spectrum of moving waves. *J. Atmos. Sci.*, **71**, 4001–4027, https://doi.org/10.1175/JAS-D-14-0095.1.

——, J. B. Edson, T. Hristov, and J. C. McWilliams, 2008: Large-eddy simulations and observations of atmospheric marine boundary layers above nonequilibrium surface waves. *J. Atmos. Sci.*, **65**, 1225–1245, https://doi.org/10.1175/2007JAS2427.1.

Sun, J., D. Vandemark, L. Mahrt, D. Vickers, T. Crawford, and C. Vogel, 2001: Momentum transfer over the coastal zone.

J. Geophys. Res., **106**, 12 437–12 488, https://doi.org/10.1029/2000JD900696.

Svensson, N., J. Arnqvist, H. Bergström, A. Rutgersson, and E. Sahlée, 2019: Measurements and modelling of offshore wind profiles in a semi-enclosed sea. *Atmosphere*, **10**, 194, https://doi.org/10.3390/atmos10040194.

Taylor, P. K., and M. A. Yelland, 2001: The dependence of sea surface roughness on the height and steepness of the waves. *J. Phys. Oceanogr.*, **31**, 572–590, https://doi.org/10.1175/1520-0485(2001)031<0572:TDOSSR>2.0.CO;2.

Vickers, D., L. Mahrt, J. Sun, and T. Crawford, 2001: Structure of offshore flow. *Mon. Wea. Rev.*, **129**, 1251–1258, https://doi.org/10.1175/1520-0493(2001)129<1251:SOOF>2.0.CO;2.

Wessel, P., J. F. Luis, L. Uieda, R. Scharroo, F. Wobbe, W. H. F. Smith, and D. Tian, 2019: The generic mapping tools version 6. *Geochem. Geophys. Geosyst.*, **20**, 5556–5564, https://doi.org/10.1029/2019GC008515.

Wyngaard, J. C., 2010: *Turbulence in the Atmosphere*. Cambridge University Press, 393 pp.